Journal of Modern Optics
Publication details, including instructions for authors and subscription information:
http://www.informaworld.com/smpp/title~content=t713191304

Dynamic coherent focus OCT with depth-independent transversal resolution

F. Lexer [a]; C. K. Hitzenberger [a]; W. Drexler [a]; S. Molebny [a]; H. Sattmann [a]; M. Sticker [a]; A. F. Fercher [a]
[a] Institute of Medical Physics, University of Vienna/Austria, Vienna, Austria

To cite this Article Lexer, F., Hitzenberger, C. K., Drexler, W., Molebny, S., Sattmann, H., Sticker, M. and Fercher, A. F.(1999) 'Dynamic coherent focus OCT with depth-independent transversal resolution', Journal of Modern Optics, 46: 3, 541 — 553
To link to this Article: DOI: 10.1080/09500349908231282
URL: http://dx.doi.org/10.1080/09500349908231282

JOURNAL OF MODERN OPTICS, 1999, VOL. 46, NO. 3, 541–553

Dynamic coherent focus OCT with depth-independent transversal resolution

F. LEXER, C. K. HITZENBERGER, W. DREXLER, S. MOLEBNY, H. SATTMANN, M. STICKER and A. F. FERCHER*

Institute of Medical Physics, University of Vienna/Austria, Waehringer Strasse 13, A-1090 Vienna, Austria

(*Received 20 August 1998*)

Abstract. We present a new OCT technique which renders the transversal resolution depth independent. This is achieved by an optical setup which shifts the focus of the beam illuminating the object through the object depth without changing the path length in the corresponding interferometer arm. Therefore, the coherence gate remains at the beam focus without any readjustment of the reference arm. Depth resolution was tested with the help of microscopy cover-plates and transversal resolution was tested with the help of Ronchi rulings. Resolution was 100 lines mm^{-1} over an object depth of 430 μm. For a first demonstration of the properties of this dynamic coherent focus scheme in a biologic system a section of a human cornea was used. We expect that this technique can further be improved to obtain transversal resolution down to the 1-μm range.

1. Introduction

Optical coherence tomography (OCT) is a new imaging technology that has found clinical application from the very beginning [1]. OCT combines partial- or low-coherence interferometry [2, 3] with scanning techniques [4–6]. It is analogous to ultrasound B mode imaging except that it uses light instead of acoustical waves. OCT can produce high-resolution cross-sectional images of transparent and semitransparent tissues. OCT has developed rapidly since its potential for application in clinical ophthalmology was demonstrated [7, 8]. An instrument for ophthalmologic application is already commercially available.

OCT can generate *in vivo* high-resolution tomograms in biological systems and can be used as a biopsy technique in a wide range of biological systems and diseases. The *in vivo* imaging of developing neural morphology and the diagnosis of the cardiovascular system have already been demonstrated [9]. High resolution and image differentiation of vascular tissues, superior to any method except excisional biopsy, was demonstrated by Brezinski *et al.* [10, 11]. OCT biopsy in human urologic tissue provided high resolution images of tissue microstructure [12]. OCT biopsy in human gastrointestinal tissue demonstrated the ability to provide *in situ* imaging of gastrointestinal microstructure with resolution near

* Corresponding author: e-mail: adolf.friedrich.fercher@univie.ac.at.

Journal of Modern Optics ISSN 0950-0340 print/ISSN 1362-3044 on line © 1999 Taylor & Francis Ltd
http://www.tandf.co.uk/JNLS/mop.htm
http://www.taylorandfrancis.com/JNLS/mop.htm

that of excisional tissue biopsy [13]. Another potential clinical field for OCT application is dermatology. One of the problems in this field is the highly scattering dry epidermis. Moistening would change its structure. Nevertheless, OCT has been demonstrated to distinguish different layers of healthy skin [14] and to distinguish melanoma maligna from healthy skin [15].

An important recent development in OCT is optical Doppler tomography [16] for analysis of internal blood flow dynamics, to monitor changes following pharmacological interventions [17], and for tissue-motion analysis [18]. Furthermore, birefringence imaging [19] has been shown to yield structural information about tissue [20] and to avoid image artifacts [21]. These techniques give access to new image parameters. Other important developments are high-speed and high-resolution OCT [22], and digital signal processing of the interferometer signal to enhance longitudinal resolution [23]. Another important development in OCT is the use of various wavelengths. For example, Bouma *et al.* have shown that longer wavelengths allow significant imaging penetration in biological tissue [24]. Longer wavelengths are of decisive importance for OCT applications in dentistry [25].

Finally, it should be mentioned that modifications of the original OCT technique have been developed: as the coherence degree is Fourier-transform related to the normalized spectral intensity [26], spectral interferometry can be used to replace the coherence scan. This can either be achieved with the help of a spectrometer or by using wavelength-tuning lasers [27–29]. Another modification has been proposed by Podoleanu *et al.* These authors use a transversal scanning method to obtain *en face* or transversal tomograms [30].

A crucial parameter of any imaging procedure is its resolution. Basically, longitudinal resolution in OCT is limited by the available bandwidth. Hence, one could simply conclude that the spectral bandwidth would have to be maximized in order to optimize depth resolution. But in case of dispersive media, like the human eye, dispersion enlarges the coherence length and consequently reduces depth resolution. Hence, apart from the dispersion balance within the interferometer, the dispersion of the object media has also to be compensated for. This, of course, cannot be done in any case. Hitzenberger *et al.* [31] have shown, that, depending on the remaining uncertainty of the object dispersion, an optimum spectral bandwidth can be found, leading to minimal coherence length and hence optimal depth resolution.

In the standard OCT technique transversal resolution is determined by the diameter of the scanning light beam. To obtain high transversal resolution a short confocal parameter must be used. This concept leads to a rather limited depth of field. In this paper we present the dynamic coherent focus technique, which renders the depth of field independent of the confocal beam parameter [32]. We start with a short description of the standard time-domain technique, and discuss logitudinal and transversal resolution in OCT.

2. Time-domain OCT

In the standard optical coherence tomography (OCT) time-domain technique the object is scanned by an object beam which forms one arm of a low coherence interferometer, as shown in figure 1. Light remitted by the object is used to synthesize the tomographic image [4]. Azimuthal positions are derived from the

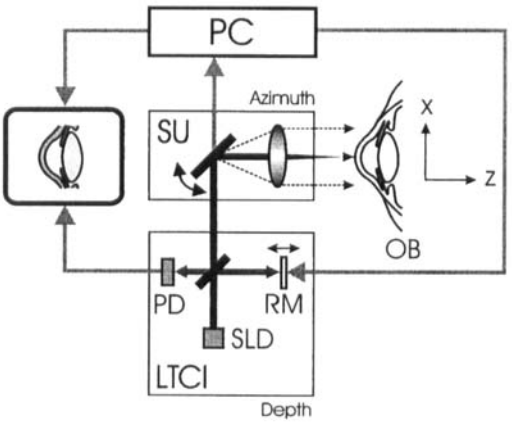

Figure 1. Standard time-domain OCT. OB = object; PD = photodetector; RM = reference mirror; SLD = superluminescent diode; SU = scanning unit. The object beam is formed by one arm of a low time-coherence interferometer (LTCI). Depth (z-)position of light remitting sites of the object is obtained from the interferometer signal generated at the photodetector by the interfering light beams reflected at the reference mirror and back-scattered from the object. The reference arm length is not shown to scale. A scanning unit (SU) is used to scan the object azimuth x.

device scanning the illuminating beam transversely across the object. Depth information is obtained by low- or partial-coherence interferometry [33]. A PC is used to control the reference mirror position and to synthesize the tomogram. Pixel positions are derived from azimuth and depth data; pixel brightness is derived from the magnitude of the photodetector signal (after some electronic processing, e.g. bandpass filtering).

Depth position of light remitting sites within the object is detected by the so-called (low-) coherence scan: The reference mirror scans along the reference beam axis. Interference occurs at the interferometer exit if the optical distance of the reference mirror to the beam splitter of the interferometer matches the distance of a light remitting site in the object arm to the beam splitter. However, it suffices if the two distances coincide within the coherence length l_C of the light (within the so-called coherence gate). Hence, l_C determines the depth resolution. An AC signal is detected by the photodetector with the Doppler frequency corresponding to the speed of the reference mirror. Therefore, noise reducing electronic AC techniques can be used to obtain high signal quality.

Let the interferometer be illuminated by a beam with the (stationary) electric field. The light intensity at the photodetector of the low time-coherence interferometer shown in figure 1 is

$$I = I_O + I_R + \varepsilon_0 c \,\mathrm{Re}\langle E_O^*(t) E_R(t+\tau)\rangle \tag{1}$$

where ε_0 is the dielectric constant, c is the velocity of light, and $\tau = 2d/c$ the time delay caused by the optical path difference $2d$ between reference and object arm. I_O, I_R are the intensities, and E_O, E_R are the electric fields returning from the object and reference arm at the photodetector. The term with the angle brackets is the first-order electric-field correlation function. This correlation

function is used to define the degree of first-order temporal coherence between the two light fields [26]:

$$g^{(1)}(t, t+\tau) = \frac{\langle E_O^*(t) E_R(t+\tau)\rangle}{[\langle |E_O(t)|^2\rangle \langle |E_R(t+\tau)|^2\rangle]^{1/2}}. \tag{2}$$

Usually in OCT light back-scattered by the object is used, as indicated in the optical scheme of figure 1. The strength of (back-) scattering is determined by the scattering potential F of the illuminated object [34]. Hence, the electric field remitted from the object arm can be expressed as a convolution of the illuminating field with the scattering potential $F(z) = -k^2 \cdot [m^2(z) - 1]$ of the object. m is the complex refractive index of the object and $k = 2\pi/\lambda$ is the wave number. Therefore the intensity at the interferometer exit is [1]:

$$I = I_O + I_R + 2(I_O I_R)^{1/2} \mathrm{Re}\left\{ g^{(1)}\left(\frac{2d}{c}\right) \otimes F(d) \right\}. \tag{3}$$

If the reference mirror is shifted with velocity v, we have at the interferometer exit:

$$I(t) = I_O + I_R + 2(I_O I_R)^{1/2} \mathrm{Re}\left\{ g^{(1)}\left(\frac{2vt}{c}\right) \otimes F(vt) \right\}. \tag{4}$$

Hence in OCT the temporal coherence degree plays the role of a spread function in depth direction. The spread function in azimuth direction is obviously given by the intensity distribution across the beam illuminating the object.

3. Dynamic coherent focus technique

We use an optical setup which shifts the focus through the object without changing the path length in the measurement arm. Therefore, the coherence gate is always at the beam focus without readjustment of the reference arm, and we have constant transversal resolution throughout the whole object depth. Part of this concept is an oscillating beam focus formed by the image of the first focus (FF in figure 2) and reflected at the oscillating mirror (SCM1 in figure 2). This oscillating beam focus is imaged into the the object by lenses O2 and O3 at a longitudinal magnification of M. A shift of the first focus by Δz is converted at the dynamic focus into a shift of $M \cdot \Delta z$. Corresponding to the shift of the dynamic focus is a change in the optical path length in the object beam. By properly selecting the magnification M this path length change can be balanced by the longitudinal shift of the dynamic focus. Hence, if the optical reference beam path length matches the optical length of the object beam up to the dynamic focus, coherence will be maintained even if the focus is shifted along the object depth.

Figure 2 shows the optical scheme of the interferometer. The beam of a fibre pigtailed superluminescent diode (SLD) is collimated by a high numerical aperture microscope lens (CL) and expanded by a Galilean telescope (GT). A nonpolarizing beamsplitter (BS1) divides the beam into reference and object beam. The measurement beam is focused at a first focus (FF) by microscope lens O1 at an oscillating scanning mirror (SCM1), positioned near the focal plane of another lens (O2). A beam deviation of $\beta - \pi$ occurs at SCM1. The beam leaving O2 enters the x–y scanning unit with scanning mirrors SCM2 and SCM3 and is focused by lens O3 into the dynamic coherent focus DCF within the object OB. The reference

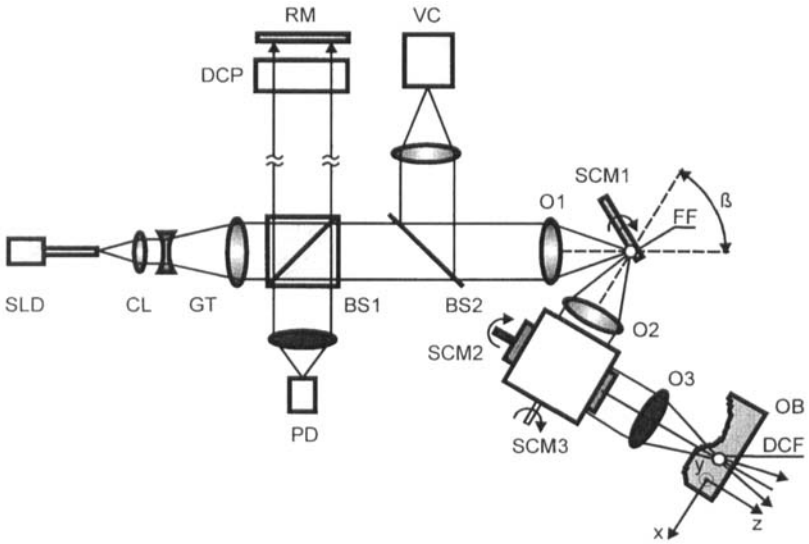

Figure 2. Optical scheme of the dynamic coherent focus interferometer. BS1, BS2 = beam splitters; CL = beam collimating lens; DCF = dynamic coherent focus; DCP = dispersion compensating plate; FF = first object beam focus; GT = Galilean telescope; O1, O2, O3 = microscope lenses; OB = object; RM = reference mirror; SCM1, SCM2, SCM3 = scanning mirrors; SLD = fibre pigtailed superluminescent diode; VC = video camera.

beam is passing a dispersion compensating plate (DCP) and is reflected at the reference mirror (RM). Both returning beams are focused onto the photodetector PD. A video camera (VC) is used to monitor the object and the position of the dynamic coherent focus.

Focusing the object beam in a medium with a refractive index different from that of air causes an additional path length mismatch. Firstly, the focus formed within the object is shifted by refraction at the interface between the air and the object surface from z to z' (see figure 3).

The position z' of the focus within the object can be obtained from a straightforward geometrical calculation. If the angle α of the focused rays within the normal to the object surface remains small, we obtain

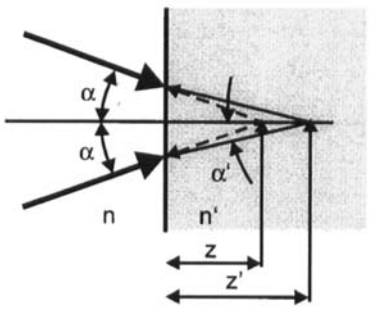

Figure 3. Focus shift due to refraction at the object surface. z = focus position in air; z' = focus position in the object; n = phase refractive index of air; n' = phase refractive index of the object.

$$z' = z \cdot \frac{\left[\left(\frac{n'}{n}\right)^2 - \sin^2 \alpha\right]^{1/2}}{\cos \alpha} \tag{5}$$

where n' equals the phase refractive index of the object. For small α and $n = 1$ we have

$$z' = n' \cdot z. \tag{6}$$

Secondly, in OCT the optical path length in a medium equals the geometrical path length times the group refractive index n_g. Hence, within the above aproximation the dynamic focus is at an optical depth of

$$z'' = n' \cdot n_g \cdot z. \tag{7}$$

If the object has a plane surface the dynamic focus is shifted by a factor of approximately $n' \cdot n_g$. In case of curved or tilted surfaces an additional walk-off of the focus will occur.

4. Resolution in OCT

Depth or longitudinal resolution in OCT is characterized by the coherence length l_C. The definition of the coherence length is based on the Fourier-uncertainty relation between the first-order degree of temporal coherence $g^{(1)}(t, t+\tau)$ and the normalized spectral distribution function

$$i(\omega) = |E(\omega)|^2 \Big/ \int_{-\infty}^{+\infty} |E(\omega)|^2 \, d\omega.$$

If the spectra of the light sources used can be approximated by Gaussian distributions, the uncertainty product of the full widths at half maximum (FWHM) of these functions is $\Delta\omega \cdot \Delta t = 8 \ln 2$ [1]. $l_C = c \cdot \Delta t$ is the coherence length, which can readily be expressed by the corresponding wavelength width $\Delta\lambda$:

$$l_C = \frac{4 \cdot \ln 2}{\pi} \cdot \frac{\lambda^2}{\Delta\lambda}. \tag{8}$$

In backscattering OCT, where light travels along the same path twice—forth and back—through the object, depth resolution equals $l_C/2$. Therefore, sometimes another definition of coherence length has been used (so-called 'round trip coherence length' $l_C/2$). At present, for example, usual superluminescent diodes at $\lambda \approx 820$ nm, have spectral widths of about $\Delta\lambda = 25$ nm. Thus, a corresponding coherence length of $l_C = 24$ μm and a depth resolution of approximately 12 μm are obtained.

Low-coherence interferometry relies on the interference of wave groups of length l_C. Hence in OCT optical distances d_o are related to geometrical distances d_g by

$$d_o = n_g \cdot d_g \tag{9}$$

where n_g is the group refractive index of the sample. Using broadband light sources to improve longitudinal resolution in measurements of dispersive media leads to a broadening of the wave group and therefore to decreased resolution [31]. The lenses used to focus the object beam generate dispersive broadening of the

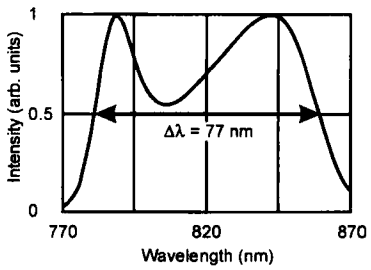

Figure 4. Emission spectrum of the superluminescent diode SLD 371 (Superlum Ltd) used in this study at nominal driving current $I = 180\,\text{mA}$.

coherence function and thus reduce longitudinal resolution. To balance this dispersion a glass plate made of BK7 40-mm thick was positioned in the reference arm of the interferometer.

In this study a pigtailed superluminescent diode SLD 371 (Superlum Ltd) was used. This diode has a centre wavelength of approximately $\lambda = 820\,\text{nm}$ and a (nominal) FWHM spectral bandwidth of $\Delta\lambda = 77\,\text{nm}$. The (nominal) coherence length of the SLD 371 is $l_C = 7.6\,\mu\text{m}$ and the corresponding depth resolution is approximately $l_C/2 = 3.8\,\mu\text{m}$.

As can be seen from figure 4, the output spectrum of the SLD 371 is not Gaussian, rather the sum of two Gaussian spectra. This double peak structure generates sidelobes in the coherence function and thus decreases longitudinal resolution. The best longitudinal resolution ($l_C/2 = 4.5\,\mu\text{m}$), i.e. the smallest FWHM of the coherence function was obtained at a driving current of 130 mA, i.e. somewhat below the nominal current.

Transversal resolution in OCT is determined by the beam-waist diameter of the scanning object beam. If the pupil of the focusing lens is uniformly filled with light the focus takes on an Airy disc intensity profile. If the pupil illumination of the focusing lens is Gaussian in profile an image spot of Gaussian profile results. If the pupil illumination has a truncated Gaussian profile a hybrid intensity profile results. In the transversal resolution experiment described below the object beam had a FWHM-intensity radius of 2.2 mm at the entrance pupil of lens O3 (NA = 0.18; 28 mm focal length). Because the NA of the focusing lens is larger than the aperture of the light beam we neglect truncation effects. This beam is focused by O3 onto the object. With an asymptotic beam divergence angle of $\varepsilon = 0.133$ the $1/e^2$-intensity radius at the focus is $w_0 = 1.97\,\mu\text{m}$, the confocal beam parameter is 15 μm.

Figure 5 demonstrates the beam quality. It shows two orthogonal intensity profiles of the focus of the object beam ($1/e^2$-diameter of 4.4 mm) obtained with a lens of 20-mm focal length immediately behind the beam expanding telescope. The focus is rather Gaussian. Besides minimal astigmatism the FWHM diameter is in agreement with the theoretical value of 2.8 μm.

In classical imaging optics the so-called Rayleigh criterion of resolution defines two incoherent points as 'barely resolved', when the centre of the Airy disc generated by one source falls on the first zero of the Airy disc generated by the second [35]. As two adjacent coherence scans are mutually incoherent we can define an analogous resolution criterion. Because of the Gaussian intensity distribution we have to replace the 'first zero of the Airy disc' by the $1/e^2$-intensity.

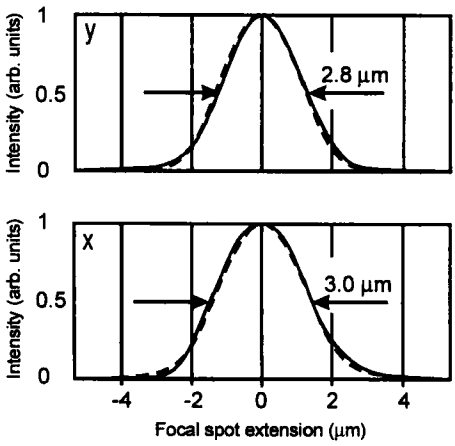

Figure 5. Quality of the intensity profile of the expanded object beam focused by a 20-mm focal length lens (immediately behind the beam expanding telescope) along the transversal x- and y-axis of the object beam focus at the object. Continuous line: actual profile. Dashed line: Gaussian profile fit.

Hence the minimum resolvable separation δ of two transversally resolved image points is defined here as the beam waist radius:

$$\delta = w_0 = \frac{\lambda}{\pi \cdot \varepsilon} \tag{10}$$

where ε is the asymptotic angle of beam divergence [36]. Furthermore, the transversal resolution in OCT depends on the position of the focus. During the coherence scan the coherence gate is shifted along the object beam. Thus, the coherence scan is in focus only within the confocal beam parameter of the illuminating beam.

Usually, to obtain reasonable depth of focus across the whole object the confocal beam parameter is chosen to match the thickness of the object to be imaged with the focus of the illuminating object beam positioned at the centre of the object depth. This strategy leads to relatively constant transversal resolution throughout the coherence scan. But, in case of thick objects, this strategy leads to a large beam waist diameter and only poor transversal resolution can be obtained. Therefore, different approaches have been used to improve transversal resolution in case of large object depth. For example, the object itself has been moved through the focus of a high NA lens to perform the coherence scan [37]. In another approach different focusing lenses have been used for imaging object structures in different depths [7]. It has also been proposed to move the focusing lens and the reference mirror by properly synchronized drives [38]. Finally, an unconventional scanning method has been used, in which reference mirror and focusing lens are mounted together on a common translation stage [39].

5. Results

In first preliminary tests coverplates used in microscopy were scanned to demonstrate depth resolution. The geometrical thickness of these slides is 130 µm. The optical thickness, as defined above, is 300 µm. Due to the beam

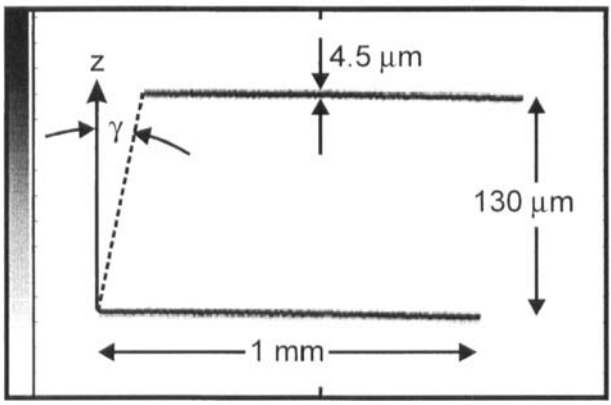

Figure 6. OCT image of a glass plate. The linear grey scale is shown at the left. The two horizontal lines indicate the anterior and posterior surface contours. γ = angle between direction of coherence scan and z-direction. Depth FWHM of the two plate surface contours = 4.5 μm.

deviation at SCM1 the dynamic focus scans the object along an axis inclined by $\gamma = 22°$ with respect to the optical axis at the object (figure 6). Though the dynamic focus is shifted along a line inclined by an angle γ with respect to the optical axis, it should be noted that the object is illuminated strictly along the optical axis in the z-direction.

In a second experiment precision Ronchi rulings were used to evaluate the transversal resolution of the DCF interferometer. We used two chrome on glass resolution targets, with 100 lines per mm on 200-μm-thick cover glass plates. The focal lengths of the lenses in the object beam were 25 mm (O1), 42 mm (O2) and 28 mm (O3). The two targets were put together along their back sides. Because of an air gap between the two glass plates the geometrical distance between the rulings turned out to be approximately 430 μm. As shown in figure 7 both rulings

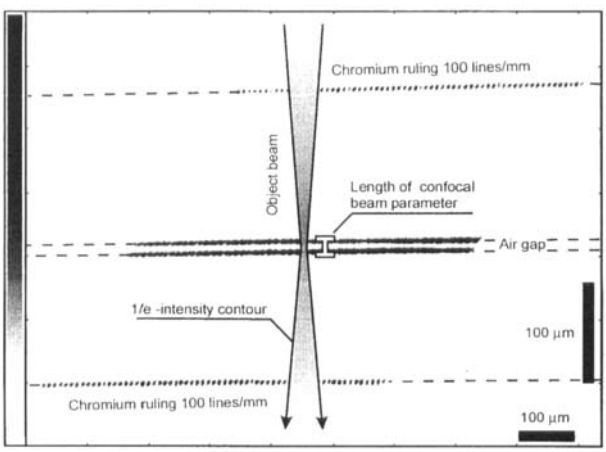

Figure 7. Tomogram of two 100 lines mm^{-1} scales separated by two glass plates. Beam waist diameter = 3.9 μm. $1/e^2$-intensity diameter at 200 μm from the beam waist apart = 54 μm.

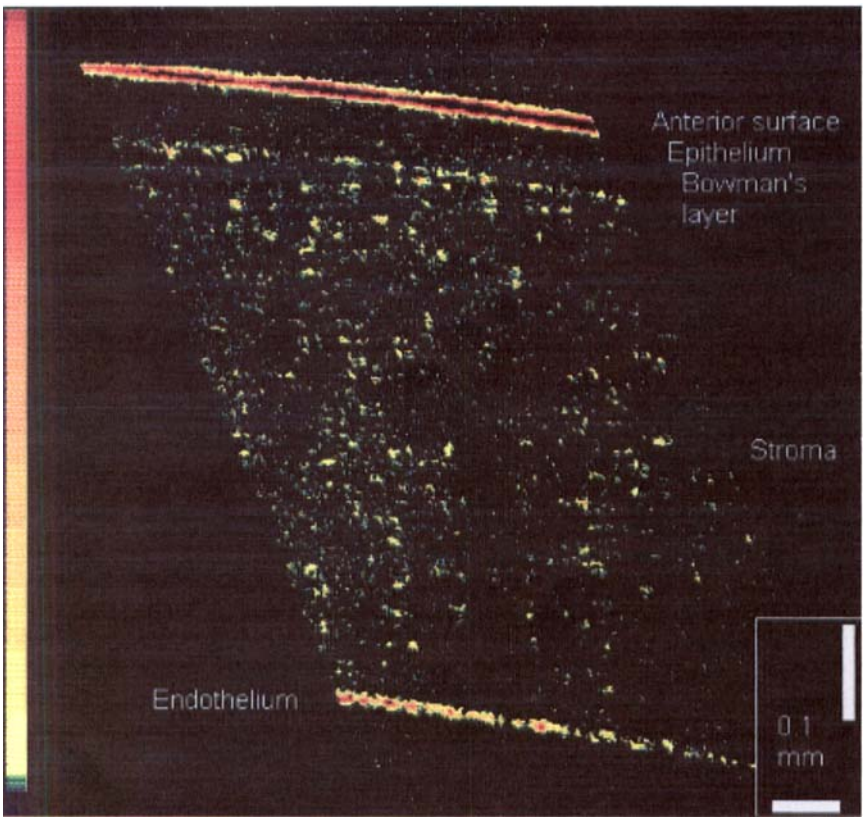

Figure 8. *In vitro* tomogram of a section of a human cornea. The anterior surface, epithelium, Bowman's layer, stroma and endothelium can be recognized.

have been clearly resolved though their period length was about one ninth that of the FWHM width of the scanning object beam (with its beam waist positioned at the opposite ruling).

For a first demonstration of the properties of the dynamic coherent focus scheme in a biologic system we used a human cornea *in vitro*. The cornea is approximately 0.5-mm thick centrally and approximately 1-mm thick peripherally. It is a layered structure consisting of the epithelium at the anterior surface, Bowman's membrane, stroma, Descemet's membrane and the endothelium at the posterior surface [40]. The epithelium represents about 10% of the corneal thickness. It typically consists of four to six layers of cells polygonal in shape, 40–60 µm in diameter and 2–6 µm thick. Adjacent is the connective tissue layer of Bowman's membrane, a homogeneous acellular layer, 10–16 µm thick. It consists of randomly arrayed collagen fibrils that merge into the more organized anterior stroma. The stroma constitutes about 90% of the corneal thickness. It is composed of intertwining lamellar collagen fibres [41]. Keratocytes are scattered with low density between the stromal lamellae. The middle and anterior third of the stroma contains nerve axons with their Schwan cells. Descemet's membrane is only loosely attached to the stroma. It is the basal lamina secreted by the endothelium, 8–10 µm thick in adulthood. The endothelium forms the posterior surface of the

cornea. It is a single layer of flattened hexagonally arranged cells, 5–6 μm thick [42]. The diameter of these cells increases with age and is 20–50 μm.

We used a peripheral section of a cornea of a 70-year-old human being. The corneal surface was kept moist with Glycerolum to prevent drying and avoid damage to the epithelium. The SLD 371 diode delivered 80 μW power at the object. The distance between two adjacent coherence scans was 3 μm. The tomogram consists of 300 pixels in the y-direction and 1000 pixels in the z-direction. (The acquisition time was 1.6 s).

The tomogram (figure 8) can be compared with the known anatomical structure of the cornea. The signal at the anterior surface is very strong due to the high difference in refractive index between air and (moistened) anterior surface. The weakly scattering layer below the anterior surface is about 75-μm thick and can be associated with the epithelium, although we cannot identify the internal cell structure. Bowman's layer is visible, and many peaks in the stroma which might be nuclei of cells (keratocytes?). At the posterior surface of the cornear a discrete structure is seen as expected from the singly layered endothelial cells.

6. Conclusion

We have presented a new OCT technique which yields transversal resolution independent of depth of field. First experiments with test targets and a human cornea confirm the scheme. Transversal resolution was demonstrated using two Ronchi gratings with 100 lines mm^{-1} separated in depth by a distance of 430 μm. This technique can also use high numerical apertures without limited depth of focus and therefore might be used to improve transversal resolution down to the 1-μm range.

Acknowledgments

The authors thank Mr L. Schachinger, from the Institute of Medical Physics, University of Vienna, for technical support, and student physicist M. Wojtkowski for his assistance in performing some of the experiments. This work was financed by the Austrian Science Foundation (FWF grant P 10316-MED).

References

[1] Fercher, A. F., 1996, *J. Biomed. Opt.*, **1**, 157–173.
[2] Fercher, A. F., and Roth, E,, 1986, *Proc. SPIE*, **658,** 48–51.
[3] Takada, K., Noda, J., and Okamoto, K., 1986, *Optics Lett.*, **11,** 680–682.
[4] Huang, D., Swanson, E. A., Lin, C. P., Schuman, J. S., Stinson, W. G., Chang, W., Hee, M. R., Flotte, T., Gregory, K., Puliafito, C. A., and Fujimoto, J. G., 1991, *Science*, **254,** 1178–1181.
[5] Fercher, A. F., Hitzenberger, C. K., Drexler, W., Kamp, G., and Sattmann, H., 1993, *Am. J. Ophthalmol.*, **116,** 113–114.
[6] Swanson, E. A., Izatt, J. A., Hee, M. R., Huang, D., Lin, C. P., Schuman, J. S., Puliafito, C. A., and Fujimoto, J. G., 1993, *Optics Lett.*, **18,** 1864–1866.
[7] Izatt, J. A., Hee, M. R., Swanson, E. A., Lin, C. P., Huang., D., Schuman, J. S., Puliafito, C. A., and Fujimoto, J. G., 1994, *Arch. Ophthalmol.*, **112,** 1584–1589.
[8] Puliafito, C. A., Hee, M. R., Lin, C. P., Reichel, E., Schuman, J. S., Duker, J. S., Izatt, J. A., Swanson, E. A., and Fujimoto, J. G., 1995, *Ophthalmol.*, **102,** 217–229.

[9] Boppart, S. A., Bouma, B. E., Brezinski, M. E., Tearney, G. J., and Fujimoto, J. G., 1996, *J. neurosci. Methods*, **70**, 65–72.
[10] Brezinski, M. E., Tearney, G. J., Bouma, B. E., Boppart, S. A., Hee, M. R., Swanson, E. A., Southern, J. F., and Fujimoto, J. G., 1996, *Am. J. Cardiol.*, **77**, 92–93.
[11] Brezinski, M. E., Tearney, G. J., Weissman, N. J., Boppart, S. A., Bouma, B. E., Hee, M. R., Weyman, A. E., Swanson, E. A., Southern, J. F., and Fujimoto, J. G., 1997, *Heart*, **77**, 397–403.
[12] Tearney, G. J., Brezinski, M. E., Southern, J. F., Bouma, B. E., Boppart, S. A., and Fujimoto, J. G., 1997, *J. Urol.*, **157**, 1915–1919.
[13] Tearney, G. J., Brezinski, M. E., Southern, J. F., Bouma, B. E., Boppart, S. A., and Fujimoto, J. G., 1997, *Am. J. Gastroent.*, **92**, 1800–1804.
[14] Lankenau, E., Welzel, J., Birngruber, R., and Engelhardt, R., 1997, *SPIE Proc.*, **2981**, 78–84.
[15] Bail, M., Eigensee, A., Häusler, G., Herrmann, J. M., and Lindener, M. W., 1997, *SPIE Proc.*, **2981**, 64–75.
[16] Chen, Z., Milner, T. E., Srinivas, S., Wang, X., Malekafzali, A., van Gemert, M. J. C., and Nelson, J. S., 1997, *Optics Lett.*, **22**, 1–3.
[17] Chen, Z., Milner, T. E., Wang, X., Srinivas, S., and Nelson, J. S., 1998, *Photochem. Photobiol.*, **67**, 1–7.
[18] Izatt, J. A., Kulkarni, M. D., Yazdanfar, S., Barton, J. K., and Welch, A. J., 1997, *Optics Lett.*, **22**, 1439–1441.
[19] de Boer, J., Milner, T. E., van Gemert, M. J. C., and Nelson, J. S., 1997, *Optics Lett.*, **22**, 934–936.
[20] Colston, B. W., Everett, M. J., and Da Silva, L. B., 1997, *Proc. SPIE*, **2973**, 216–220.
[21] Everett, M. J., Schoenenberger, K., Colston, B. W., and Da Silva, L. B., 1998, *Optics Lett.*, **23**, 228–230.
[22] Bouma, B. E., Tearney, G. J., Boppart, S. A., Golubovic, B., Bilinski, I. B., Brezinski, M. E., and Fujimoto, J. G., 1997, *SPIE Proc.*, **2981**, 37–44.
[23] Kulkarni, M., and Izatt, J. A., 1997, *SPIE Proc.*, **2981**, 2–6.
[24] Bouma, B. E., Nelson, L. E., Tearney, G. J., Jones, D. J., Brezinski, M. E., and Fujimoto, J. G., 1998, *J. biomed. Optics*, **3**, 76–79.
[25] Colston, B. W., Everett, M. J., Da Silva, L. B., Otis, L. L., Stroeve, P., and Nathel, H., 1998, *Appl. Optics*, **27**, 3582–3585.
[26] Loudon, R., 1985, *The Quantum Theory of Light* (Oxford: Clarendon Press).
[27] Fercher, A. F., Hitzenberger, C. K., Drexler, W., Kamp, G., Strasser, I., and Li, H. C., 1993, *In vivo optical coherence tomography in ophthalmology*. In *Medical Optical Tomography: Functional Imaging and Monitoring*, edited by B. Chance *et al.*, Vol. IS 11. (Bellingham: SPIE Press), pp. 355–370.
[28] Bail, M., Häusler, G., Herrmann, J. M., Lindner, M. W., and Ringler, R., 1996, *SPIE Proc.*, **2925**, 298–303.
[29] Chinn, S. R., Swanson, E. A., and Fujimoto, J. G., 1997, *Optics Lett.*, **22**, 340–342.
[30] Podoleanu, A. Gh., Dobre, G. M., Webb, D. J., and Jackson, D. A., 1996, *Optics Lett.*, **21**, 1789–1791.
[31] Hitzenberger, C. K., Drexler, W., Baumgartner, A., and Fercher, A. F., 1997, *SPIE Proc.*, **2981**, 29–36.
[32] Lexer, F., Fercher, A. F., Sattmann, H., Drexler, W., Molebny, S., 1998, *Proc. SPIE*, **3251**, 85–90.
[33] Fercher, A. F., Hitzenberger, C., Juchem, M., 1991, *J. mod. Opt.*, **38**, 1327–1333.
[34] Wolf, E., 1969, *Optics Commun.*, **1**, 153–156.
[35] Goodman, J. W., 1969, *Introduction to Fourier Optics* (New York: McGraw-Hill).
[36] Gerrard, A., and Burch, J. M., 1975, *Introduction to Matrix Optics Methods in Optics* (London: Wiley).
[37] Izatt, J. A., Hee, M. R., Owen, G. M., Swanson, E. A., and Fujimoto, J. G., 1994, *Optics Lett.*, **19**, 590–592.
[38] Swanson, E., 1992, Patent publication US PCT/US92/03536.
[39] Schmitt, J. M., Lee, S. L., and Yung, K. M., 1997, *Optics Commun.*, **142**, 203–207.

[40] KLYCE, S., and BEUERMAN, R. W., 1998, in *The Cornea*, edited by Kaufman, H. E., Barron, B. A., and McDonald, M. B., 2nd edn (Boston: Butterworth-Heinemann).
[41] VAUGHAN, D., and ASBURY, T., 1983, *General Ophthalmology*, 10th edn (Los Altos: Lange Medical Publications).
[42] FINE, B. S., and YANO, M., 1979, *Ocular Histology*, 2nd edn (Hagerstown: Harper & Row).